Research Article | Vol. 9, No. 7 / 1 July 2019 / Optical Materials Express 3115
Optical Materials EXPRESS

Optical pulse structuring in gas-filled hollow-core kagomé PCF for generation and detection of phase-locked multi-THz pulses [Invited]

ALEXEI HALPIN, NICOLAS COUTURE, AND JEAN-MICHEL MÉNARD*

Department of Physics, University of Ottawa, 25 Templeton Street, Ottawa, Ontario K1N 6N5, Canada
**jean-michel.menard@uottawa.ca*

Abstract: A gas-filled hollow-core photonic crystal fiber is used to structure near-infrared ultrashort pulses and enable the generation and time-resolved detection of multi-terahertz radiation. Due to self-phase modulation, near-infrared pulses launched into the fiber experience spectral broadening characterized by the appearance of side lobes at the edges of the spectrum. Phase-locked terahertz generation between 10 and 18 terahertz is achieved by difference-frequency mixing of these spectral side lobes. This method allows for an implementation of time-resolved spectroscopy in the multi-terahertz range through the efficient production of near-infrared pulses with tailored spectra, without requiring ultrabroadband optical sources.

1. Introduction

Field-resolved spectroscopies represent an ever-growing research domain, allowing to overcome the restrictions of intensity-based measurements through phase-sensitive detection. In the terahertz (THz) spectral range, such techniques have previously been leveraged to great success for measuring the complex conductivity of photoexcited systems [1], allowing for contact-free probes of free and bound carriers in optoelectronic materials including bulk [2] or nanostructured inorganic semiconductors [3], organic systems [4,5], as well as novel materials such as monolayer transition metal dichalcogenides [6]. More recently, the increased access to few- or even sub-cycle fields in the multi-THz (> 10 THz) range has opened new avenues for ultrabroadband probes of materials across enormous spectral ranges using nonlinear crystals [7–10] or plasma-based sources [11,12]. Such sources have been applied to studies of the quantum vacuum [13,14], the spectroscopy of excitonic dynamics in perovskites [15] and two-dimensional materials [16], as well as the dynamics of phase transitions measured using ultrafast nanoscopy [17].

The sources employed in these impressive spectroscopic results exploit difference-frequency generation (DFG) from ultrashort near-infrared (NIR) pulses in nonlinear crystals. This process results in broadband THz pulses that are phase-locked with the NIR fields for performing time-domain spectroscopy. The continued development of these techniques has been facilitated in part by the increasing bandwidth of available pump sources. By definition, the frequencies produced using DFG depend directly on those contained in the associated pump fields. However, most commercially available laser sources, such as Yb:KGW sources, offer bandwidths of 5 THz or less. As such, the realization of broadband pulses at multi-THz frequencies or higher have instead been generated using bulky Ti:Sapphire amplifiers or other specialized sources [9,18]. An alternative approach, aiming to maximize the generation efficiency for specific frequency ranges in the > 10 THz range or in the mid-infrared (MIR), has relied on mixing two separate frequency-detuned pulses in nonlinear crystals [19,20]. Overall, these implementations either rely on the use of lasers with uniquely large bandwidths, or hinge on the nontrivial combination of multiple sources such as parametric amplifiers.

#360713 https://doi.org/10.1364/OME.9.003115
Journal © 2019 Received 22 Feb 2019; revised 4 Jun 2019; accepted 7 Jun 2019; published 25 Jun 2019

Optical Materials EXPRESS

Meanwhile, in the optical and NIR domains, the maturation of hollow-core fiber-based technologies has provided researchers with an inherently flexible tool for achieving spectral broadening and self-compression for various sources [21–23]. Contrary to regular solid-core fibers, these specialty fibers can be filled with a gaseous medium. This provides tunability of the linear and nonlinear optical properties of the fiber, through the selection of gas along with its pressure in the fiber. The capability of hollow-core photonic crystal fibers (HC-PCF) to transmit high peak fields is also desirable for many nonlinear optical applications.

As a result of the tight and relatively long confinement of optical pulses in gas-filled HC-PCFs, self-phase modulation (SPM) can be used to broaden the spectrum of NIR pulses possessing relatively low-energy in the μJ range [24–26]. Moreover, the HC-PCF can operate in the negative dispersion regime [25–27], an added feature to achieve a short pulse duration at the output of the fiber. Therefore, the use of a HC-PCF allows to extend the capabilities of narrowband femtosecond laser sources towards broadband and ultrashort optical applications such as phase-locked multi-THz generation and detection.

In this article we present an instrument for multi-THz spectroscopy based on SPM inside an Ar-filled HC-PCF. We use gallium selenide (GaSe) as a material for THz generation and detection due to favorable phase matching conditions for accessing the multi-THz region. The key operating principle of the instrument relies on the action of SPM in the HC-PCF, which causes spectral broadening and the appearance of side lobes at the edges of the NIR spectrum. The two lobes are separated in the frequency domain, where this spectral separation follows the strength of the SPM in the fiber. Following subsequent DFG in GaSe, we demonstrate tuning of the central THz frequency generated between 10 and 18 THz. This frequency can be tuned in a facile manner through external control of the amount of SPM in the gas-filled HC-PCF via the gas pressure or injected NIR pulse energy. Using an HC-PCF in this way provides high-throughput and flexible access to this portion of the THz spectrum for researchers relying on femtosecond laser sources with a < 5 THz bandwidth.

2. Experiment

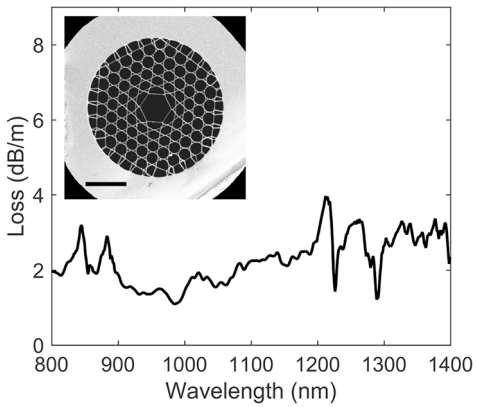

Fig. 1. Measured loss spectrum of the HC-PCF, showing low losses in the vicinity of the wavelengths of interest in these experiments. Inset: electron micrograph of the cross-section of the fiber, showing the kagomé lattice and 34 μm-diameter core (scale bar of 50 μm).

The ultrafast optical source consists of a commercially available Yb:KGW amplifier delivering 180 fs pulses centered at 1035 nm at a repetition rate of 1.1 MHz. These pulses are coupled into a 55 cm-long kagomé HC-PCF with a 34 μm-diameter core (side-to-side). The measured loss-spectrum of the fiber used in these experiments in Fig. 1 shows relatively low losses of

Optical Materials EXPRESS

< 2 dB/m over the spectral range of 900-1100 nm used in our experiment. The two-dimensional structure of the photonic crystal defining the fiber can be seen in the electron micrograph in the inset of Fig. 1. The fiber is entirely placed inside a gas cell which is then filled with Ar gas. In the fiber the pulses undergo SPM, a $\chi^{(3)}$ effect, which leads to the generation of new frequencies through the intensity dependent refractive index of Ar. By changing the gas pressure inside the HC-PCF or the input pulse energy, we can control the amount of SPM. Here, we apply a constant Ar pressure of 13 bar, to provide sufficient SPM at different pulse energies. Under these experimental conditions, the calculated zero-dispersion wavelength (ZDW) occurs at 650 nm and the group velocity dispersion (GVD) is -6 fs^2/cm. After passing through the HC-PCF, the pulse is sent to a chirped mirror pair (CMP) that compensates for GVD, leading to nearly transform-limited NIR pulses entering the THz section of the setup. In this work, the CMP corrects for approximately -2200 fs^2.

A conventional THz time-domain spectroscopy (THz-TDS) scheme is used to generate and detect THz radiation with the structured NIR pulses [28]. The full experimental setup is shown in Fig. 2. Following spectral shaping in the HC-PCF, the beam is split into two paths. In the first path, THz radiation is generated via DFG in a 30 (± 10) µm thick GaSe crystal, and it is subsequently focused into a similar GaSe crystal for detection. Meanwhile, the beam in the second path acts as a gate pulse for time-resolved detection of the multi-THz pulse. The gate pulse, which can be temporally delayed using a translation stage, is spatially and temporally overlapped with the THz pulse in the detection crystal. Time-resolved electro-optic sampling (EOS) is performed to directly measure the oscillating electric field of the THz radiation.

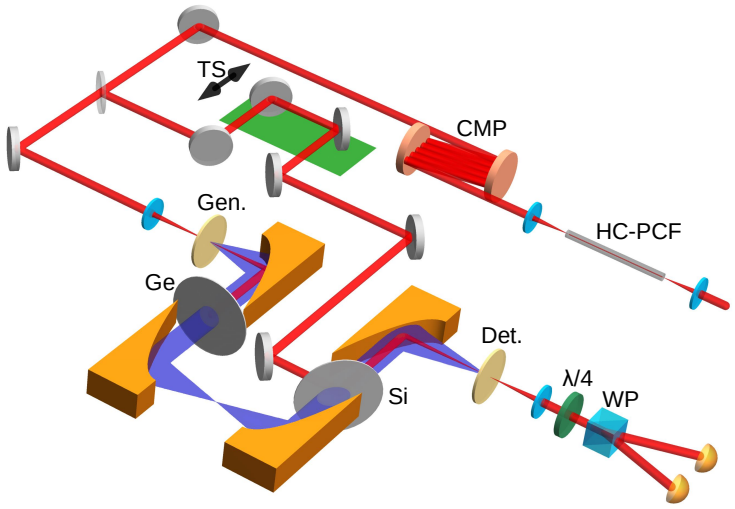

Fig. 2. Schematic of the experimental setup. Ultrashort NIR pulses are coupled into a HC-PCF filled with 13 bar of Ar gas. THz radiation is subsequently generated and detected using a standard THz-TDS system. CMP: chirped mirror pair; TS: translation stage; Gen.: generation crystal; Ge: germanium wafer; Si: silicon wafer; Det: detection crystal; λ/4: quarter-wave plate; WP: Wollaston prism.

3. Results and discussion

Figure 3 shows the measured NIR spectral amplitudes and autocorrelation traces of the pulse at the output of the HC-PCF for different input pulse energies. The amplitudes are obtained from the intensity spectra measured with a USB spectrometer while the temporal profiles are measured with a home-made intensity autocorrelator utilizing second harmonic generation (SHG) from a

Optical Materials EXPRESS

150-μm-thick beta-barium borate (BBO) crystal. We display the spectra in Fig. 3(a) in amplitude, rather than in intensity, as the THz generation efficiency from the DFG process depends on the spectral field amplitudes. Directly at the output of the optical source, the "reference'' NIR amplitude spectrum has a bandwidth of approximately 4 THz full-width-half-maximum (FWHM). The spectrum is strongly modified by nonlinear propagation inside the HC-PCF. We observe a gradual spectral broadening as we increase the input pulse energy from 0.7 μJ to 2.2 μJ. For pulse energies above 0.9 μJ, the NIR spectral energy is mostly redistributed within two side lobes at the edges of the spectrum while the amplitude significantly decreases around the central frequency. From the spectroscopic measurements shown in Fig. 3(a), we determine that the side lobe separation increases from 4.5 THz to 24 THz for the lowest to highest pulse energies considered here.

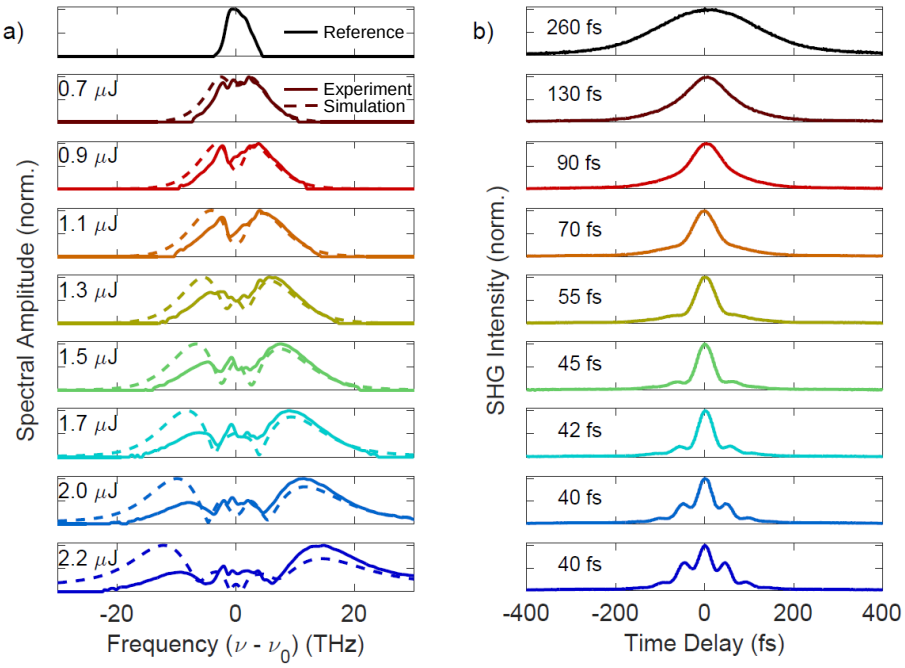

Fig. 3. (a) Measured NIR spectra (plotted in amplitude) following broadening in the HC-PCF through SPM for increasing pulse energies injected into the fiber and (b) their corresponding measured intensity autocorrelation traces. The full-width-half-maximum (FWHM) of the autocorrelation traces are displayed. The spectral and temporal profiles of the reference pulse, before entering the HC-PCF, are shown in the top panels in black. Solid lines represent experimental data while dashed lines are simulations. The spectra are re-centered about the central frequency of the laser.

In order to model the spectral response of the HC-PCF we performed simulations solving the nonlinear wave equation for a Gaussian input spectrum [29], where the fiber dispersion is approximated by that of a narrow-bore capillary [30] and SPM is applied via the addition of a nonlinear spectral phase. For the pulse duration and input coupling used in our experimental conditions we find reasonable agreement between the simulations and the experimental results. Some discrepancies nevertheless remain due to the non-Gaussian spectral shape of our input pulse, and due to residual third-order chirp which is not compensated by the grating compressor in the amplified laser system.

The autocorrelation (AC) traces shown in Fig. 3(b) demonstrate the consequences of the SPM and CMP on the temporal profile of the NIR pulses. While broadband spectra are required for

Optical Materials EXPRESS

efficient DFG at multi-THz frequencies, short NIR pulses are also crucial to achieve (i) broadband THz generation, since relevant frequencies involved in the DFG process overlap in time, and (ii) for time-domain detection, since the gating pulse must be shorter than the period of the oscillating THz field. The "reference" NIR pulse in Fig. 3(b) yields an AC trace with a 260 fs FWHM, which corresponds to a 180 fs pulse duration assuming a Gaussian temporal shape. For an input pulse energy of 0.7 μJ, propagation through the HC-PCF and post-compression stage in the CMP reduces the pulse duration by half. We then further shorten the NIR pulses by another factor of three by increasing the input pulse energy up to 1.7 μJ. At that pulse energy we approach the resolution limit of our autocorrelator. The shortest pulse measured yields an AC trace of 40 fs corresponding to a pulse duration of ~30 fs. The non-Gaussian shape of the AC trace at the highest pulse energies is due to an imperfect spectral phase compensation by the CMP. Nonetheless, the NIR pulses are measured to be sufficiently short to achieve THz generation and detection over the frequency range considered in our experiments (< 20 THz).

Figures 4(a) and 4(b) show measured time-resolved THz transients and their associated amplitude spectra, respectively. For clarity we have normalized each trace and its spectrum to their maximal value. In the top panel, we show a THz measurement obtained with the NIR "reference" pulse. We observe an oscillatory electric field transient at low frequencies, where the amplitude spectrum presents a narrow peak in the vicinity of 4 THz, consistent with the bandwidth of our laser source. In contrast, when a HC-PCF is used, we observe a rapidly oscillating field in the time-domain, corresponding to frequencies generated beyond 4 THz, with a gap in the vicinity of 5-7 THz within the Reststrahlen band of GaSe [31].

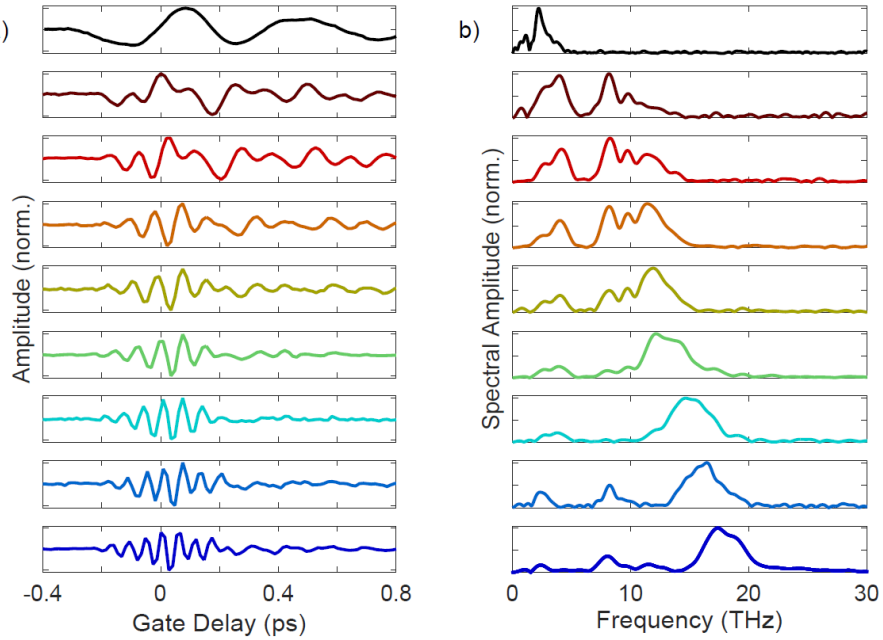

Fig. 4. (a) THz transients and (b) spectra corresponding to the pulse energies given in Fig. 3. In the top panels we show the measured THz transient and spectrum corresponding to the reference NIR pulse before entering the HC-PCF. For low pulse-energies injected into the HC-PCF the time-domain traces contain mostly low-frequency oscillations. For higher pulse energies, the field transients shorten considerably, and the high-frequency components of the transient become more evident in the spectral domain.

Optical Materials EXPRESS

For increasing NIR pulse energy the transients shorten, and begin to resemble a few-cycle pulse with high-frequency oscillations. Correspondingly, we observe the emergence of more high-frequency content in the THz amplitude spectra plotted in Fig. 4(b). By varying the input pulse energy launched into the HC-PCF, we can smoothly tune the maximum generated THz frequency from 10 to 18 THz. This frequency tuning is the direct result of the NIR spectral and temporal reshaping, which provides access to high THz frequencies by enabling nonlinear interaction between a larger range of NIR spectral components. Furthermore, the redistribution of the NIR spectral weight into two separated side lobes allows us to target a particular THz frequency. The dominant side lobes of the structured NIR pulse possess unequal amplitudes, however, the optical energy contained within the two dominant side lobes can be maximized by adjusting the high-order dispersion of the input pulse before entering the HC-PCF, according to numerical simulations. This scheme would then result in a more efficient THz generation in the high-frequency regime, and may even be able to compete with more complex configurations relying on a dual beam geometry [19,20].

We do not explore the regime above 20 THz, however, due to technical limitations in controlling the spectral phase of the SPM-broadened pulses following the HC-PCF: the CMP employed in this work only compensates for dispersion over a range of approximately 20 THz, which is narrower than the largest NIR bandwidth shown in the bottom panel of Fig. 3(a). For increasing bandwidths, achieving transform-limited pulses to allow for effective generation and detection of THz pulses requires a more precise approach to dispersion compensation [32]. With suitably compressed broadband pulses, there is no fundamental limitation restricting our approach from reaching higher frequencies into the MIR.

4. Conclusion

The use of NIR pulses undergoing SPM in a gas-filled HC-PCF is shown to provide a platform for the generation of tunable multi-THz pulses in the range of 10-18 THz using a compact Yb:KGW system. In our experiment, the structured NIR pulses have spectra characterized by two side lobes, which can be separated in frequency by an arbitrary amount determined by the input pulse energy. Alternatively, one could also keep the input pulse energy constant and instead vary the gas pressure inside the HC-PCF to modulate the spectral broadening [28]. Compensating for linear chirp using a CMP decreases the time duration of the SPM-broadened pulses following propagation in the HC-PCF, as verified through autocorrelation measurements. The central THz frequency generated using the associated ultrashort NIR pulses can thus be controlled between 10-20 THz by exploiting SPM, through DFG between the associated side lobes in the NIR spectrum.

Reaching higher THz frequencies above 20 THz also demands a more broadband compensation of dispersion after the HC-PCF. Nevertheless, we believe that our general fiber-based scheme does not impose any fundamental limitations for achieving higher generation frequencies into the MIR, and can potentially be used with various ultrafast optical sources. We expect this configuration, leveraging the robust technology of nonlinear photonics in fibers and the use of compact Yb:KGW laser systems, to be widely applicable and easily multiplexed for enabling THz spectroscopy covering the full multi-THz range.

Finally, by combining PCF and THz technologies, this work is even more relevant in the recent context of emerging HC-PCFs able to transmit MIR and THz radiation [33–37]. In the future, it could also be integrated with a design enabling second-order nonlinear effects in HC-PCF, allowing an all-fiber configuration for tunable phase-locked THz generation by DFG [38,39].

Funding

Natural Sciences and Engineering Research Council of Canada (NSERC); Canada Foundation for Innovation (CFI); Ontario Ministry of Research, Innovation and Science (MRIS).

Optical Materials EXPRESS

Acknowledgments

We thank the Russell division (Max Planck Institute for the Science of Light) for providing the kagomé PCF and Prof. David Cooke (McGill University) for providing GaSe crystals.

References

1. R. Ulbricht, E. Hendry, J. Shan, T. F. Heinz, and M. Bonn, "Carrier dynamics in semiconductors studied with time-resolved terahertz spectroscopy," Rev. Mod. Phys. **83**(2), 543–586 (2011).
2. M. C. Beard, G. M. Turner, and C. A. Schmuttenmaer, "Terahertz spectroscopy," J. Phys. Chem. B **106**(29), 7146–7159 (2002).
3. P. Parkinson, C. Dodson, H. J. Joyce, K. A. Bertness, N. A. Sanford, L. M. Herz, and M. B. Johnston, "Noncontact Measurement of Charge Carrier Lifetime and Mobility in GaN Nanowires," Nano Lett. **12**(9), 4600–4604 (2012).
4. F. A. Hegmann, R. R. Tykwinski, K. P. H. Lui, J. E. Bullock, and J. E. Anthony, "Picosecond Transient Photoconductivity in Functionalized Pentacene Molecular Crystals Probed by Terahertz Pulse Spectroscopy," Phys. Rev. Lett. **89**(22), 227403 (2002).
5. E. Hendry, M. Koeberg, J. Schins, H. Nienhuys, V. Sundström, L. Siebbeles, and M. Bonn, "Interchain effects in the ultrafast photophysics of a semiconducting polymer: THz time-domain spectroscopy of thin films and isolated chains in solution," Phys. Rev. B **71**(12), 125201 (2005).
6. C. J. Docherty, P. Parkinson, H. J. Joyce, M.-H. Chiu, C.-H. Chen, M.-Y. Lee, L.-J. Li, L. M. Herz, and M. B. Johnston, "Ultrafast Transient Terahertz Conductivity of Monolayer MoS_2 and WSe_2 Grown by Chemical Vapor Deposition," ACS Nano **8**(11), 11147–11153 (2014).
7. R. A. Kaindl, F. Eickemeyer, M. Woerner, and T. Elsaesser, "Broadband phase-matched difference frequency mixing of femtosecond pulses in GaSe: Experiment and theory," Appl. Phys. Lett. **75**(8), 1060–1062 (1999).
8. R. Huber, A. Brodschelm, F. Tauser, and A. Leitenstorfer, "Generation and field-resolved detection of femtosecond electromagnetic pulses tunable up to 41 THz," Appl. Phys. Lett. **76**(22), 3191–3193 (2000).
9. C. Kübler, R. Huber, S. Tübel, and A. Leitenstorfer, "Ultrabroadband detection of multi-terahertz field transients with GaSe electro-optic sensors: Approaching the near infrared," Appl. Phys. Lett. **85**(16), 3360–3362 (2004).
10. A. Sell, A. Leitenstorfer, and R. Huber, "Phase-locked generation and field-resolved detection of widely tunable terahertz pulses with amplitudes exceeding 100 MV/cm," Opt. Lett. **33**(23), 2767–2769 (2008).
11. E. Matsubara, M. Nagai, and M. Ashida, "Ultrabroadband coherent electric field from far infrared to 200 THz using air plasma induced by 10 fs pulses," Appl. Phys. Lett. **101**(1), 011105 (2012).
12. V. A. Andreeva, O. G. Kosareva, N. A. Panov, D. E. Shipilo, P. M. Solyankin, M. N. Esaulkov, P. González de Alaiza Martínez, A. P. Shkurinov, V. A. Makarov, L. Bergé, and S. L. Chin, "Ultrabroad Terahertz Spectrum Generation from an Air-Based Filament Plasma," Phys. Rev. Lett. **116**(6), 063902 (2016).
13. C. Riek, D. V. Seletskiy, A. S. Moskalenko, J. F. Schmidt, P. Krauspe, S. Eckart, S. Eggert, G. Burkard, and A. Leitenstorfer, "Direct sampling of electric-field vacuum fluctuations," Science **350**(6259), 420–423 (2015).
14. C. Riek, P. Sulzer, M. Seeger, A. S. Moskalenko, G. Burkard, D. V. Seletskiy, and A. Leitenstorfer, "Subcycle quantum electrodynamics," Nature **541**(7637), 376–379 (2017).
15. D. A. Valverde-Chavez, C. S. Ponseca, C. C. Stoumpos, A. Yartsev, M. G. Kanatzidis, V. Sundström, and D. G. Cooke, "Intrinsic femtosecond charge generation dynamics in single crystal $CH_3NH_3PbI_3$," Energy Environ. Sci. **8**(12), 3700–3707 (2015).
16. P. Steinleitner, P. Merkl, P. Nagler, J. Mornhinweg, C. Schüller, T. Korn, A. Chernikov, and R. Huber, "Direct Observation of Ultrafast Exciton Formation in a Monolayer of WSe_2," Nano Lett. **17**(3), 1455–1460 (2017).
17. M. A. Huber, M. Plankl, M. Eisele, R. E. Marvel, F. Sandner, T. Korn, C. Schüller, R. F. Haglund, R. Huber, and T. L. Cocker, "Ultrafast Mid-Infrared Nanoscopy of Strained Vanadium Dioxide Nanobeams," Nano Lett. **16**(2), 1421–1427 (2016).
18. I. Pupeza, D. Sánchez, J. Zhang, N. Lilienfein, M. Seidel, N. Karpowicz, T. Paasch-Colberg, I. Znakovskaya, M. Pescher, W. Schweinberger, V. Pervak, E. Fill, O. Pronin, Z. Wei, F. Krausz, A. Apolonski, and J. Biegert, "High-power sub-two-cycle mid-infrared pulses at 100 MHz repetition rate," Nat. Photonics **9**(11), 721–724 (2015).
19. M. Knorr, J. Raab, M. Tauer, P. Merkl, D. Peller, E. Wittmann, E. Riedle, C. Lange, and R. Huber, "Phase-locked multi-terahertz electric fields exceeding 13 MV/cm at a 190 kHz repetition rate," Opt. Lett. **42**(21), 4367 (2017).
20. M. Seidel, X. Xiao, S. A. Hussain, G. Arisholm, A. Hartung, K. T. Zawilski, P. G. Schunemann, F. Habel, M. Trubetskov, V. Pervak, O. Pronin, and F. Krausz, "Multi-watt, multi-octave, mid-infrared femtosecond source," Sci. Adv. **4**(4), eaaq1526 (2018).
21. P. St. J. Russell, P. Hölzer, W. Chang, A. Abdolvand, and J. C. Travers, "Hollow-core photonic crystal fibres for gas-based nonlinear optics," Nat. Photonics **8**(4), 278–286 (2014).
22. T. Balčiūnas, C. Fourcade-Dutin, G. Fan, T. Witting, A. A. Voronin, A. M. Zheltikov, F. Gerome, G. G. Paulus, A. Baltuška, and F. Benabid, "A strong-field driver in the single-cycle regime based on self-compression in a kagome fibre," Nat. Commun. **6**(1), 6117 (2015).
23. G. Fan, T. Balčiūnas, T. Kanai, T. Flöry, G. Andriukaitis, B. E. Schmidt, F. Légaré, and A. Baltuška, "Hollow-core-waveguide compression of multi-millijoule CEP-stable 32 μm pulses," Optica **3**(12), 1308 (2016).

Optical Materials EXPRESS

24. C. Schriber, C. J. Saraceno, C. F. Dutin, F. Benabid, F. Emaury, F. Gerome, M. Trant, O. H. Heckl, T. Südmeyer, U. Keller, and Y. Y. Wang, "Beam delivery and pulse compression to sub-50 fs of a modelocked thin-disk laser in a gas-filled Kagome-type HC-PCF fiber," Opt. Express **21**(4), 4986–4994 (2013).
25. J. C. Travers, W. Chang, J. Nold, N. Y. Joly, and P. St. J. Russell, "Ultrafast nonlinear optics in gas-filled hollow-core photonic crystal fibers [Invited]," J. Opt. Soc. Am. B **28**(12), A11–A26 (2011).
26. M. Gebhardt, C. Gaida, S. Hädrich, F. Stutzki, C. Jauregui, J. Limpert, and A. Tünnermann, "Nonlinear compression of an ultrashort-pulse thulium-based fiber laser to sub-70 fs in Kagome photonic crystal fiber," Opt. Lett. **40**(12), 2770 (2015).
27. K. F. Mak, M. Seidel, O. Pronin, M. H. Frosz, A. Abdolvand, V. Pervak, A. Apolonski, F. Krausz, J. C. Travers, and P. St. J. Russell, "Compressing μJ-level pulses from 250 fs to sub-10 fs at 38-MHz repetition rate using two gas-filled hollow-core photonic crystal fiber stages," Opt. Lett. **40**(7), 1238–1241 (2015).
28. W. Cui, A. W. Schiff-Kearn, E. Zhang, N. Couture, F. Tani, D. Novoa, P. St. J. Russell, and J.-M. Ménard, "Broadband and tunable time-resolved THz system using argon-filled hollow-core photonic crystal fiber," APL Photonics **3**(11), 111301 (2018).
29. G. Agrawal, *Nonlinear Fiber Optics* (Elsevier, 2013).
30. E. Marcatili and R. Schmeltzer, "Hollow metallic and dielectric waveguides for long distance optical transmission and lasers," Bell Syst. Tech. J. **43**(4), 1783–1809 (1964).
31. C.-S. Chang, C.-W. Chen, C.-L. Pan, J. Y. Huang, P.-K. Chung, S.-T. Yen, S.-H. Lin, and T.-T. Tang, "Optical properties and potential applications of e-GaSe at terahertz frequencies," J. Opt. Soc. Am. B **26**(9), A58–A65 (2009).
32. R. L. Fork, C. H. Cruz, P. C. Becker, and C. V. Shank, "Compression of optical pulses to six femtoseconds by using cubic phase compensation," Opt. Lett. **12**(7), 483–485 (1987).
33. K. Nielsen, H. K. Rasmussen, A. J. L. Adam, P. C. Planken, O. Bang, and P. U. Jepsen, "Bendable, low-loss Topas fibers for the terahertz frequency range," Opt. Express **17**(10), 8592–8601 (2009).
34. J. Anthony, A. Argyros, R. Leonhardt, and S. G. Leon-Saval, "THz propagation in kagome hollow-core microstructured fibers," Opt. Express **19**(19), 18470–18478 (2011).
35. A. N. Kolyadin, A. F. Kosolapov, A. D. Pryamikov, A. S. Biriukov, V. G. Plotnichenko, and E. M. Dianov, "Light transmission in negative curvature hollow core fiber in extremely high material loss region," Opt. Express **21**(8), 9514 (2013).
36. J. Yang, J. Zhao, C. Gong, H. Tian, L. Sun, P. Chen, L. Lin, and W. Liu, "3D printed low-loss THz waveguide based on Kagome photonic crystal structure," Opt. Express **24**(20), 22454 (2016).
37. H. Li, G. Ren, B. Zhu, Y. Gao, B. Yin, J. Wang, and S. Jian, "Guiding terahertz orbital angular momentum beams in multimode Kagome hollow-core fibers," Opt. Lett. **42**(2), 179 (2017).
38. J.-M. Ménard and P. St. J. Russell, "Phase-matched electric-field-induced second-harmonic generation in Xe-filled hollow-core photonic crystal fiber," Opt. Lett. **40**(15), 3679–3682 (2015).
39. J.-M. Ménard, F. Köttig, and P. St. J. Russell, "Broadband electric-field-induced LP_{01} and LP_{02} second harmonic generation in Xe-filled hollow-core PCF," Opt. Lett. **41**(16), 3795–3798 (2016).